Dalton Transactions

PAPER

View Article Online
View Journal | View Issue

Cite this: *Dalton Trans.*, 2016, **45**, 5223

Synthesis of borocarbonitride from a multifunctional Cu(I) boron imidazolate framework†

Tian Wen, Er-Xia Chen, De-Xiang Zhang and Jian Zhang*

Received 9th December 2015,
Accepted 8th February 2016

DOI: 10.1039/c5dt04805b

www.rsc.org/dalton

A functional Cu(I) boron imidazolate framework (BIF) with a ladder-chain structure can not only change to another single-chain structure by incorporating 4,4′-bipyridine, but can also act as a reducing agent to load trimetal Au–Ag–Pd nanoparticles directly; the BIF with loaded noble NPs showed an excellent reduction effect on 4-nitrophenol. Moreover, we obtained a porous borocarbonitride by the direct carbonisation of this low-dimensional BIF. The resulting porous borocarbonitride exhibits fast adsorption behavior for 4-nitrophenol and can be a high-temperature conductor.

The last two decades have witnessed fast development in coordination polymers (CPs) because of their interesting structural features and applications, such as loading nanoparticles (NPs), photoluminescence and catalysis.[1–3] The main challenge being faced is the reasonable design of CPs with multifunctional properties. A large amount of CPs that show exceptional catalysis effects have been successfully applied to various catalytic reactions.[4] However, the catalysis of ligand-functionalized CPs is at an initial stage, although post-synthetic strategies have been employed as another efficient way to introduce certain functional groups.[5] Moreover, some CPs can perform structural transformations *via* crystal-to-crystal or amorphous-to-crystal transformations. However, solvent-assisted structural transformations *via* crystal disassembly and reassembly are rarely investigated.[6]

Though CPs showed some advantages above, CPs derived from carbon materials are little explored up to now. Actually, carbon materials have triggered much more attention due to their porous structure for applications in the purification and storage of gases, and catalysis.[7–9] In addition, doping carbon materials with boron gives them potential in applications such as those requiring good electrical properties and gas sensors.[10,11] The synthesis methodology of borocarbonitride ($B_xC_yN_z$) materials involves a carbonisation process. For example, Antonietti and co-workers obtained boron carbon nitrides from the pyrolysis of graphitic carbon nitride.[12] The Qiao group reported metal–organic frameworks (MOFs) as precursors for the synthesis of porous carbon and carbon nitride materials.[13] A nanoporous borocarbonitride was also prepared by Maji and Rao by the carbonisation of high-dimensional boron-based MOFs with auxiliary naphthalenedicarboxylate ligands.[14] However, synthetic protocols for $B_xC_yN_z$ are rarely reported.[15,16]

In our initial study, we mainly focused on 4-connected boron imidazolate frameworks (BIFs).[17] As a result, a series of high-dimensional BIFs with tetrahedral Cu^+ ions were successfully constructed, but low-dimensional and functionalized BIFs based on tridentate boron imidazolate ligands are still rarely explored. 3-Connected boron imidazolate ligands have redox-active properties and may directly reduce monometal or bimetal nanoparticles into their frameworks; this is attributed to the presence of rich B–H functional bonds from the ligands.[18]

Here, we report two Cu(I/II) BIFs, [CuBH(dm-bim)$_3$] (**BIF-36**) and $Cu_2(AB)_2$(BH(dm-bim)$_3$)$_2$(bipy) (**BIF-37**; bipy = 4,4′-bipyridine). Notably, **BIF-36** with a ladder-chain structure undergoes redox-triggered structural transformation to **BIF-37** with a single-chain structure by incorporating 4,4′-bipyridine in the solvent, which is visible to the naked-eye. Moreover, **BIF-36** acts as a reducing agent to load trimetal Au–Ag–Pd nanoparticles directly. Furthermore, we obtained for the first time a porous borocarbonitride, by the direct carbonisation of **BIF-36**, which exhibits promising properties, such as being a high temperature conductor and fast adsorption for 4-nitrophenol.

Experimental section

Materials and instrumentation

All reagents were purchased commercially and used without further purification. All syntheses were carried out in a 20 mL

State Key Laboratory of Structural Chemistry, Fujian Institute of Research on the Structure of Matter, Chinese Academy of Sciences, Fuzhou, Fujian 350002, P. R. China. E-mail: zhj@fjirsm.ac.cn; Fax: +86-591-83715030; Tel: +86-591-83715030

†Electronic supplementary information (ESI) available: Powder XRD patterns, TGA data and cif file. CCDC 1057285 (**BIF-36**) and 1057286 (**BIF-37**). For ESI and crystallographic data in CIF or other electronic format see DOI: 10.1039/c5dt04805b

vial under autogenous pressure. Diffraction data were collected using an Oxford SuperNova diffractometer with graphite monochromated Cu Kα radiation (λ = 0.71073 Å) at 293 K. The structure was solved using direct methods and refined by the full-matrix least-squares technique using SHELXTL.[5] All Powder X-ray diffraction (PXRD) analyses were recorded using a Rigaku Dmax2500 diffractometer with Cu Kα radiation (λ = 1.54056 Å) with a step size of 0.05°. Thermal stability studies were carried out on a NETSCHZ STA-449C thermoanalyzer with a heating rate of 10 °C min^{-1} under a nitrogen atmosphere. Fluorescence spectra were measured using a HORIBA Jobin-Yvon FluoroMax-4 spectrometer. The synthesized borocarbonitride sample was ground and then mixed with a suitable amount of ethanol to form a paste. Subsequently the paste was coated onto the Ag–Pd interdigital electrodes of the sensor substrates purchased from Beijing Elite Tech Co., Ltd.

Synthesis of BIF-36. KBH(dm-bim)$_3$ (dm-bim = 5,6-dimethylbenzimidazolate) (0.1 mmol), 4,4′-bipyridine (0.1 mmol), and CuI (0.1 mmol) were dissolved in 6 mL of DMF/(+/−)2-amino-1-butanol (AB)/CH_3CN (1 : 1 : 1, v/v; DMF = *N*,*N*-dimethylformamide; CH_3CN = acetonitrile) mixed solvent. Then, the solution was sealed in a 20 mL vial. The mixture was heated at 100 °C for 2 days and then cooled to room temperature. Colorless block crystals were formed and collected by filtration and then washed with water several times (yield: ~55% based on the KBH(dm-bim)$_3$ ligands).

Synthesis of nanoporous borocarbonitride. BIF-36 (300 mg) was kept in a silica boat and then carbonised at 450 °C under N_2 atmosphere for 6 h at a heating rate of 3 °C min^{-1} and then it was maintained for 6 h. Finally, the resulting pyrolyzed compound was cooled in a furnace at a cooling rate of 1 °C min^{-1}. Borocarbonitride was obtained after the removal of surface species using HCl (20%); it was then filtered and subsequently washed several times with a water–ethanol mixture and dried at 100 °C. The purity of the sample was confirmed using several methods such as FT-IR, XPS, elemental analysis and microscopic techniques.

Crystal data for BIF-36. $C_{57}H_{56}B_2Cu_2N_{13}O$, M = 1087.87, Monoclinic, a = 28.7669(6) Å, b = 9.4653(2) Å, c = 20.6970(5) Å, α = 90°, β = 104.402(2)°, γ = 90°, V = 5458.4(2) Å^3, T = 293(2) K, space group $I2/a$, Z = 8, 5493 reflections measured, 4559 independent reflections (R_{int} = 0.0575). The final R_1 value was 0.0470 ($I > 2\sigma(I)$). The final wR (F^2) value was 0.1031 ($I > 2\sigma(I)$). The goodness of fit on F^2 was 1.035. Elemental analyses for **BIF-36**: calcd (%): C 62.87, H 5.14, N 16.72, found: C 62.83, H 5.28, N 16.31.

Crystal data for BIF-37. $C_{36}H_{52}BCuN_8O_2$, M = 703, Triclinic, a = 12.3677(12) Å, b = 12.7886(12) Å, c = 14.2243(13) Å, α = 109.825(9)°, β = 115.576(9)°, γ = 96.582(8), V = 1816.5(4) Å^3, T = 293(2) K, space group $P\bar{1}$, Z = 16 397 reflections measured, 3449 independent reflections (R_{int} = 0.0615). The final R_1 value was 0.0939 ($I > 2\sigma(I)$). The final wR (F^2) value was 0.2503 ($I > 2\sigma(I)$). The goodness of fit on F^2 was 1.014. Elemental analyses for **BIF-37**: calcd (%): C 61.45, H 7.3, N 15.93, found: C 61.00, H 6.92, N 15.71.

Results and discussion

Reversible structural transformation

Single-crystal X-ray diffraction analysis shows that **BIF-36** crystallizes in the monoclinic space group $I2/a$. The pure phase of **BIF-36** has been demonstrated using powder X-ray diffraction (PXRD). The crystalline sample of **BIF-36** is insoluble in common solvents (*e.g.* DMF, ethanol and acetonitrile). The thermogravimetric analysis (TGA) reveals that there is no obvious weight loss before 300 °C (Fig. S1†). In **BIF-36**, the μ_2-BH(dm-bim)$_3^-$ ligands link the 3-coordinate Cu^+ centers into a ladder-like chain (Fig. 1a).

When the crystals of **BIF-36** in the mother liquid were placed at room temperature for two months, their color changed to blue (Fig. 1c). The X-ray diffraction result confirmed that **BIF-36** was converted into **BIF-37**. Interestingly, **BIF-37** cannot be synthesized by the direct reaction of 4,4′-biprymidine, AB, CuI and BH(dm-bim)$_3$-ligands. **BIF-37** crystallizes in the triclinic space group $P\bar{1}$. The pure phase and the stability of **BIF-37** have been characterized using powder X-ray diffraction (PXRD) and thermogravimetric analysis (TGA), respectively (Fig. S2–3†). In **BIF-37**, each Cu^{2+} center displays a pentagonal pyramidal coordination geometry, and two neighboring Cu^{2+} ions are chelated to two AB ligands. The BH(dm-bim)$_3^-$ ligand only acts as the ending ligand and bonds to the Cu^{2+} center. The resulting $Cu_2(AB)_2(BH(dm\text{-}bim)_3)_2$ units are bridged by 4,4′-bipyridine to form a chain (Fig. 1b).

In addition, the transformation can be reversed from **BIF-37** to **BIF-36** by placing **BIF-37** in the mother liquid at

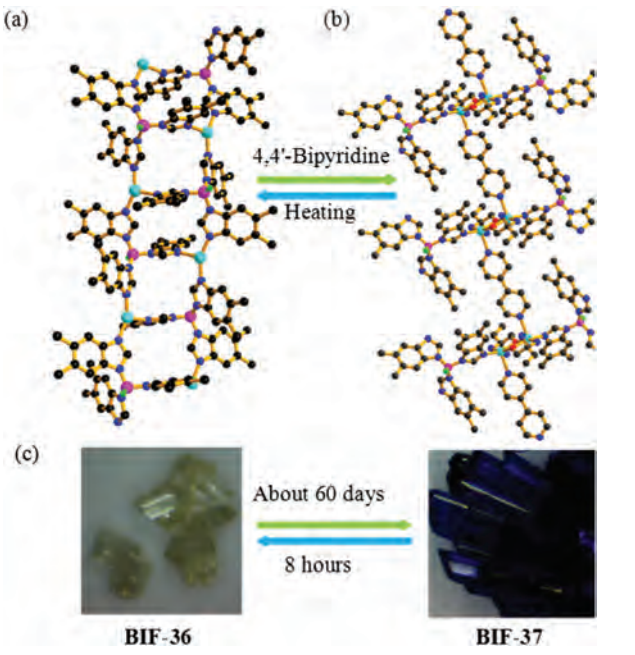

Fig. 1 (a) The ladder-like chain in **BIF-36** and (b) the single chain in **BIF-37**. Color codes: Cu, blue; B, purple; C, black; N, blue; H, green; and partial H atoms are omitted for clarity. (c) Photo of as-synthesized samples of **BIF-36** (colorless) and **BIF-37** (blue).

100 °C for 8 hours. We believe herein that the oxygen from air acts as the oxidant in the process of structural transformation. In order to confirm such an assumption, we carried out the following control experiments. When **BIF-36** was suspended in the mother liquid under N_2 atmosphere at room temperature for two months, **BIF-36** remained intact. As well as oxygen, (+/−)2-amino-1-butanol medium is also essential for this transformation. When **BIF-36** was immersed in other kinds of ROH solvents, such as CH_3OH, C_2H_5OH or i-PrOH, the structural transformation was not observed.

Loading trimetal nanoparticles

Due to the presence of B–H bonds from the $BH(dm\text{-}bim)_3^-$ ligands, the redox activity of **BIF-36** was investigated. **BIF-36** could serve as the reducing agent and contribute to the direct formation of Au nanoparticles in the **BIF-36** crystals. Fortunately, we obtained **Au–Ag–Pd@BIF-36** by a two-step process. Firstly, fresh **BIF-36** crystals (120 mg) were immersed in a mixed water solution of $HAuCl_4$ (20 mmol L^{-1}, 4 ml) and $HPdCl_4$ (20 mmol L^{-1}, 4 ml) for 5 hours at room temperature to produce **Au–Pd@BIF-36**. The color change of the **BIF-36** crystals from colorless to wine-colored may be due to the surface plasmons of the spherical noble metal Au and Pd nanoparticles (Fig. S4b†). The field-emission (FE) TEM image of the resulting **Au–Pd@BIF-36** sample indicated the formation of **Au–Pd** bimetal NPs in the crystals. After that, the **Au–Pd@BIF-36** crystals were filtered out and washed three times with water and ethanol, respectively, and then put into a water solution of $AgNO_3$ (5 mmol L^{-1}, 6 ml) at room temperature to prepare trimetal nanoparticles. After 12 hours, the color of the **Au–Pd@BIF-36** crystals eventually becomes gray-black, indicating the formation of trimetal nanoparticles (Fig. S4c†). Meanwhile, TEM images of the **BIF-36** sample indicated the formation of **Au–Ag–Pd** trimetal NPs in the crystals (Fig. 2a–c).

From studying further information on the composition of the **BIF-36** loaded with noble metals, the X-ray photoelectron spectra (XPS) as well as the energy-dispersive X-ray spectroscopy (EDS) (Fig. 3) data indicated that Au(0), Pd(0) and Ag(0) coexist in the solid (Fig. S5–7†). Moreover, the lattice fringe spacings of the trimetal Au–Ag–Pd NPs were measured to be 0.232 nm, 0.221 nm and 0.235 nm, which match the *d* values for Ag(111), Pd(111) and Au(111), respectively. Furthermore, mapping images and line scanning profiles showed the full incorporation of AgPd alloy nanocrystals (NCs) into the **BIF-36** (Fig. 2d). The powder X-ray diffraction (PXRD) patterns further reveal that the framework of the **Au–Ag–Pd@BIF-36** is retained after the loading of the trimetal noble NPs (Fig. 4). Compared with other external reducing agents employed for the reduction of noble metal ions, these results exhibit that BIFs with functional B–H bonds have advantages for producing trimetal noble nanoparticles directly.

Catalytic activity of Au–Ag–Pd@BIF-36

The properties of **Au–Ag–Pd@BIF-36** were investigated. The reduction of 4-nitrophenol was chosen as a model reaction. The reaction was monitored using UV-vis absorption spectro-

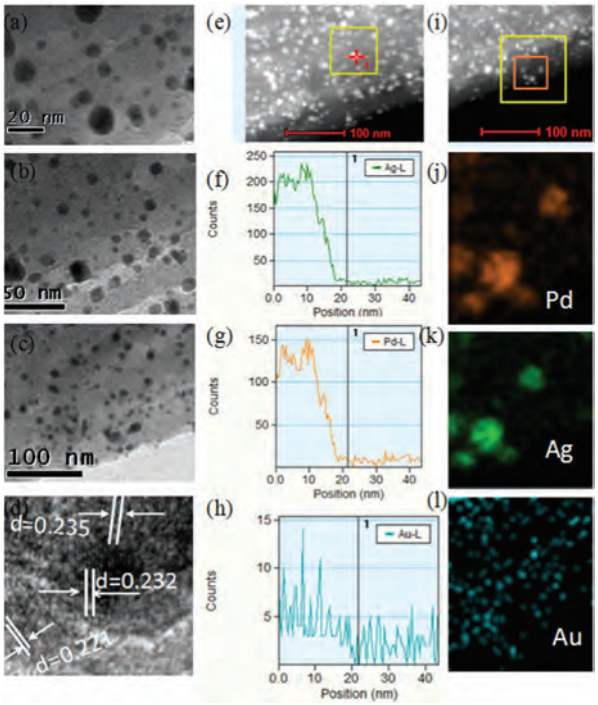

Fig. 2 (a), (b) and (c) Typical TEM images of the prepared **Au–Ag–Pd@BIF-36** at different magnifications. (d) HRTEM image of **Au–Ag–Pd@BIF-36**. (e), (f), (g) and (h) Line scanning profiles of the **Au–Ag–Pd** NPs encapsulated in **BIF-36**. (i), (j), (k) and (l) Mapping images of Ag, Pd and Au.

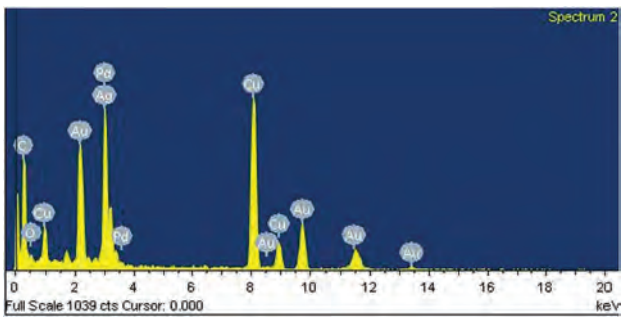

Fig. 3 EDS spectrum of **Au–Ag–Pd@BIF-36**.

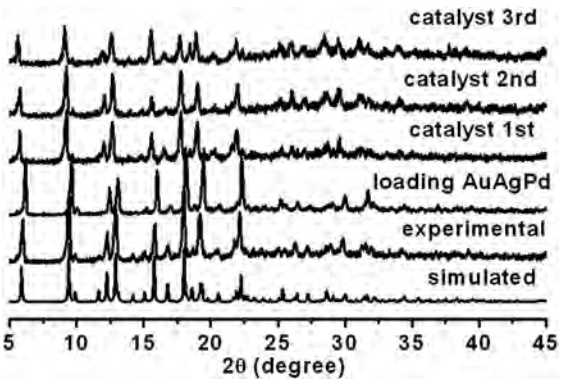

Fig. 4 The PXRD patterns of **BIF-36** under different conditions.

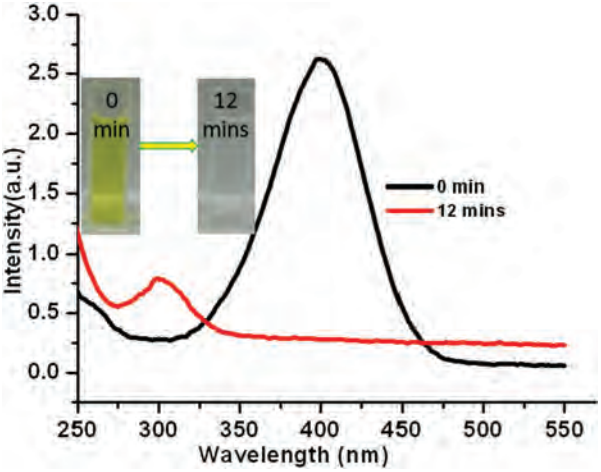

Fig. 5 UV-vis spectra showing the reduction of 4-nitrophenol over **Au–Ag–Pd@BIF-36** (the inset shows photographic images of the color change of the 4-nitrophenol solution).

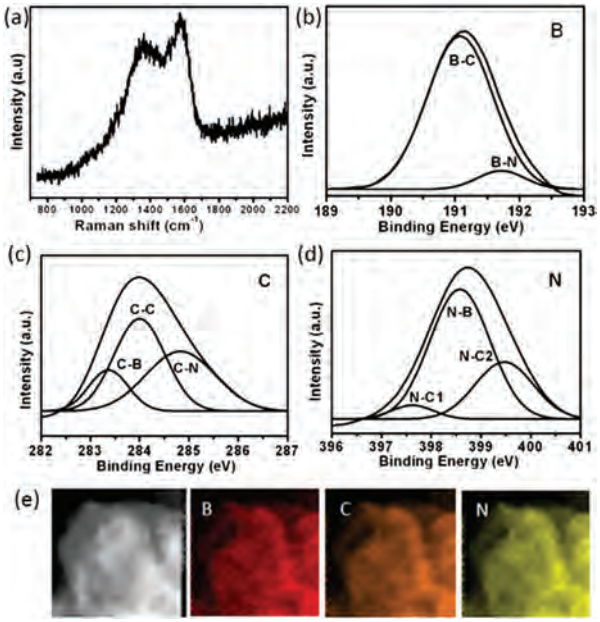

Fig. 6 (a) Raman spectrum of the resultant borocarbonitride derived from **BIF-36**. (b), (c) and (d) X-ray photoelectron spectroscopy (XPS) spectra of the resultant borocarbonitride. (e) Mapping images of B, C and N.

scopy. The absorption of 4-nitrophenol at 400 nm significantly declined along with a concomitant increase of the ~300 nm peak of 4-aminophenol (Fig. 5). To study the reusability, three recycles of the catalytic reaction were tested for the same **Au–Ag–Pd@BIF-36** catalyst. The catalyst showed similar catalytic activity without obvious changes in the conversion for the same reaction time (Fig. S8†), suggesting the stability of the samples. Further, TEM measurements of the catalysts indicated that the size of the **Au–Ag–Pd@BIF-36** NPs almost remained the same after the reaction (Fig. S9†). These results suggest that **Au–Ag–Pd@BIF-36** serving as a catalyst reducing organic molecules is feasible.

Derived mesoporous borocarbonitride

We have employed **BIF-36** as the precursor for the synthesis of a borocarbonitride at 450 °C. The samples, after carbonisation, were dissolved and washed in a solution of HCl and water–ethanol mixture, respectively. The pure phase of borocarbonitride has been demonstrated using powder X-ray diffraction (PXRD) (Fig. S10†). The thermogravimetric analysis reveals that there was an obvious weight loss before 800 °C (Fig. S11†). The Raman spectrum shows bands at 1340 (D-band) and 1593 cm^{-1} (G-band), the latter being characteristic of sp^2 sheet structures (Fig. 6a). The FT-IR spectrum of the borocarbonitride (Fig. S12–13†) exhibits a broad band around 3440–3304 cm^{-1} due to the stretching modes of the N–H group. The peaks at 1612 and 2194 cm^{-1} are due to C=C and C=N stretching, respectively. The peaks at 1619 and 1382 cm^{-1} are due to –C=C– and –C=N– stretching, respectively. Peaks at 1295 and 829 cm^{-1} correspond to in-plane B–N and out-of-plane B–N–B vibrations, respectively. X-ray photoelectron spectroscopy (XPS) measurements show sharp signals for B, C and N atoms (Fig. 6b–d). The B 1s signal can be deconvoluted into two peaks at 191.6 and 192.1 eV, which are assigned to B–C and B–N, respectively. The C 1s signal can be deconvoluted into three peaks with binding energies 283.1, 285.4 and 289.2 eV, which are assigned to C–B, C–C and C–N, respectively. The N 1s spectrum shows three peaks centred at 398.4, 401.1 and 402.7 eV, respectively.

Transmission electron microscope (TEM) (Fig. 7a and b) and field-emission scanning electron microscope (FE-SEM) (Fig. 7c) images of borocarbonitride show the BNC with a hollow interior. The high-resolution TEM images suggest a porous nature, with a size of 50 nm. Energy-dispersive X-ray spectra (Fig. S14†) and mapping images clearly show the presence of B, C and N atoms (Fig. 6e). The HRTEM elemental

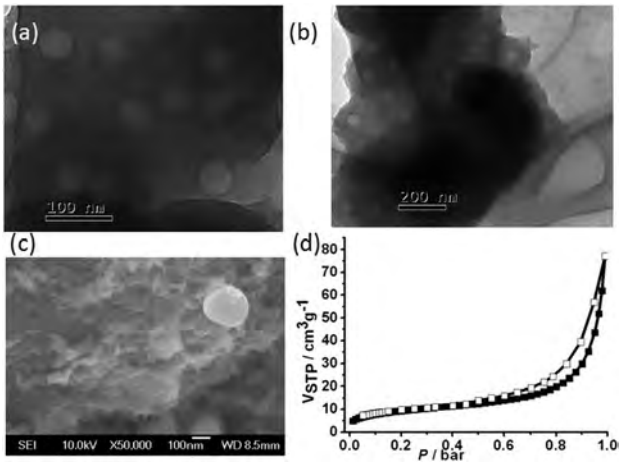

Fig. 7 (a), (b) and (c) Typical TEM images of the resultant borocarbonitride derived from **BIF-36** at different magnifications. (d) The N_2 adsorption–desorption isotherms of the resultant borocarbonitride.

mapping shows homogeneous distributions of the elements throughout the sample. Based on the demonstrated inductively coupled plasma atomic emission spectroscopy (ICP-AES), elemental analysis, and XPS results, the composition of the borocarbonitride is found to be $B_{2.94}C_{3.41}N_{0.79}$. Fig. 6d displays the N_2 adsorption–desorption isotherms of $B_{2.94}C_{3.41}N_{0.79}$, which are typical of type-II isotherms.[19] The Brunauer–Emmett–Teller (BET) and Langmuir surface areas of the sample are about 33.30 and 51.43 $m^2\ g^{-1}$, respectively, and the borocarbonitride exhibits a small pore volume of 0.12 $cm^3\ g^{-1}$.

Qualities of borocarbonitride materials

The borocarbonitride material, on the one hand, showed excellent adsorption efficiency of 4-nitrophenol (4-NP) in aqueous solution at room temperature. For the adsorption of 4-NP, the characteristic absorption of 4-NP at about 400 nm was selected to monitor the adsorption process. After 5 min, the adsorption amount of 4-NP reached almost 99.99% (Fig. S15†). On the other hand, the borocarbonitride material exhibited a unique property of being a high-temperature conductor. The borocarbonitride material was fabricated into an interdigitated electrode to estimate the electrical conductivity of the material. As illustrated in Fig. 8a, the ohmic value is so high ($\geq 2.0 \times 10^9\ \Omega$) that it can be regarded as insulated when the operating temperature is lower than 300 °C. However, there is a large change in the ohmic value when the operating temperature exceeds 300 °C. It is noteworthy that the response–recovery time is rapid when the temperature changes (Fig. 8b), which suggests that the borocarbonitride material may act as a current switch.

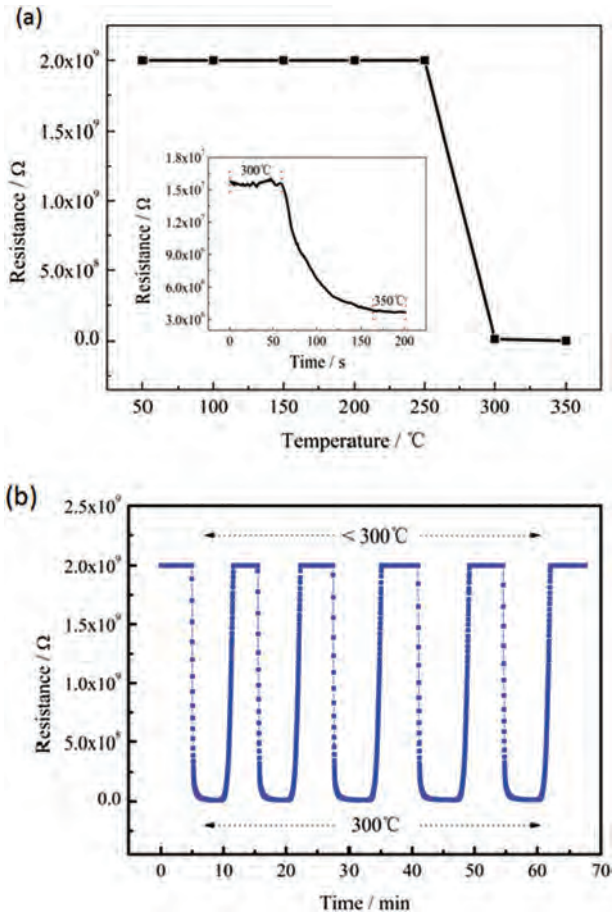

Fig. 8 (a) The resistance of the borocarbonitride material changing along with the operating temperature (the inset shows resistance variation in the range of 300–350 °C); (b) the response–recovery curve of the material with the change of operating temperature.

Conclusions

In this work, a multifunctional Cu(I) compound (**BIF-36**) was successfully constructed and characterized, and showed reversible structural transformation involving valence change. **BIF-36** also can load trimetal nanoparticles directly and form alloy nanocrystals at ambient temperature for the catalysis of the reduction of 4-nitrophenol. Moreover, a mesoporous borocarbonitride was obtained by direct carbonisation of the low-dimensional **BIF-36**. These convincing results indicated the structural diversity and multiple functions of low-dimensional BIF materials.

Acknowledgements

We thank the support of this work by 973 program (2012CB821705), NSFC (21221001) and CAS (XDA07070200).

Notes and references

1 Q. L. Zhu and Q. Xu, *Chem. Soc. Rev.*, 2014, **43**, 5468.
2 (*a*) Z. C. Hu, B. J. Deibert and J. Li, *Chem. Soc. Rev.*, 2014, **43**, 5815; (*b*) Y. J. Cui, Y. F. Yue, G. D. Qian and B. L. Chen, *Chem. Rev.*, 2012, **112**, 1126.
3 (*a*) A. Dhakshinamoorthy and H. Garcia, *Chem. Soc. Rev.*, 2014, **43**, 5750; (*b*) M. Yoon, R. Srirambalaji and K. Kim, *Chem. Rev.*, 2012, **112**, 1196.
4 (*a*) J. Liu, L. Chen, H. Cui, J. Zhang, L. Zhang and C. Y. Su, *Chem. Soc. Rev.*, 2014, **43**, 6011; (*b*) T. Wen, D.-X. Zhang, J. Liu, R. Lin and J. Zhang, *Chem. Commun.*, 2013, **49**, 5660; (*c*) Y. L. Hou, R. W. Y. Sun, X. P. Zhou, J. H. Wang and D. Li, *Chem. Commun.*, 2014, **50**, 2295.
5 (*a*) S. M. Cohen, *Chem. Rev.*, 2012, **112**, 970; (*b*) D. J. Lun, G. I. N. Waterhouse and S. G. Telfer, *J. Am. Chem. Soc.*, 2011, **133**, 5806.
6 (*a*) J. Y. Ge, J. C. Wang, J. Y. Cheng, P. Wang, J. P. Ma, Q. K. Liu and Y. B. Dong, *Chem. Commun.*, 2014, **50**, 4434; (*b*) D. Liu, M. Li and D. Li, *Chem. Commun.*, 2009, 6943.
7 (*a*) L. L. Liu, C. X. Yu, F. J. Ma, Y. R. Li, J. J. Han, L. Lin and L. F. Ma, *Dalton Trans.*, 2015, **44**, 1636; (*b*) X. Feng, R. F. Li, L. Y. Wang, S. W. Ng, G. Z. Qin and L. F. Ma, *CrystEngComm*, 2015, **17**, 7878; (*c*) Y. Zhao, D. S. Deng, L. F. Ma, B. M. Ji and L. Y. Wang, *Chem. Commun.*, 2013, **49**, 10299;

(*d*) J. Lee, J. Kim and T. Hyeon, *Adv. Mater.*, 2006, **18**, 2073.

8 G. P. Mane, S. N. Talapaneni, C. Anand, S. Varghese, H. Iwai, Q. Ji, K. Ariga, T. Mori and A. Vinu, *Adv. Funct. Mater.*, 2012, **22**, 3596.

9 Y. Zhai, Y. Dou, D. Zhao, P. F. Fulvio, R. T. Mayes and S. Dai, *Adv. Mater.*, 2011, **23**, 4828.

10 D. Portehault, C. Giordano, C. Gervais, I. Senkovska, S. Kaskel, C. Sanchez and M. Antonietti, *Adv. Funct. Mater.*, 2010, **20**, 1827.

11 A. Thomas, A. Fischer, F. Goettmann, M. Antonietti, J. O. Muller, R. Schlogl and J. M. Carlsson, *J. Mater. Chem.*, 2008, **18**, 4893.

12 (*a*) Y. Wang, X. Wang and M. Antonietti, *Angew. Chem., Int. Ed.*, 2012, **51**, 68; (*b*) X. Wang, X. Chen, A. Thomas, X. Fu and M. Antonietti, *Adv. Mater.*, 2009, **21**, 1609.

13 T. Y. Ma, S. Dai, M. Jaroniec and S. Z. Qiao, *J. Am. Chem. Soc.*, 2014, **136**, 13925.

14 K. Jayaramulu, N. Kumar, A. Hazra, T. K. Maji and C. N. R. Rao, *Chem. – Eur. J.*, 2013, **19**, 6966.

15 W. L. Wang, X. D. Bai, K. H. Liu, Z. Xu, D. Golberg, Y. Bando and E. G. Wang, *J. Am. Chem. Soc.*, 2006, **128**, 6530.

16 S. H. Jhi and Y. K. Kwon, *Phys. Rev.*, 2004, **69**, 245407.

17 (*a*) F. Wang, Y.-B. Shu, J. Zhang and X. Bu, *Chem. – Eur. J.*, 2012, **18**, 11876; (*b*) J. Zhang, T. Wu, C. Zhou, S. Chen, P. Feng and X. Bu, *Angew. Chem., Int. Ed.*, 2009, **48**, 2542; (*c*) H.-X. Zhang, H.-R. Fu, H.-Y. Li, J. Zhang and X. Bu, *Chem. – Eur. J.*, 2013, **19**, 11527; (*d*) H. X. Zhang, F. Wang, H. Yang, Y. X. Tan, J. Zhang and X. Bu, *J. Am. Chem. Soc.*, 2011, **133**, 11884.

18 (*a*) H. X. Zhang, M. Liu, X. Bu and J. Zhang, *Sci. Rep.*, 2014, **4**, 3923; (*b*) T. Wen, D. X. Zhang, H. X. Zhang, H. B. Zhang, J. Zhang and D. S. Li, *Chem. Commun.*, 2014, **50**, 8754; (*c*) T. Wen, D. X. Zhang, J. Liu, H. X. Zhang and J. Zhang, *Chem. Commun.*, 2015, **51**, 1353.

19 (*a*) K. S. W. Sing, *Pure Appl. Chem.*, 1985, **57**, 603; (*b*) J. Rouquerol, D. Avnir, C. W. Fairbridge, D. H. Everett, J. M. Haynes, N. Pernicone, J. D. F. Ramsay, K. S. W. Sing and K. K. Unger, *Pure Appl. Chem.*, 1994, **66**, 1739.